bio-protocol

Open Access

Published: Apr 05, 2023

In situ Microinflammation Detection Using Gold Nanoclusters and a Tissue-clearing Method

Fayrouz Naim[1, 2, #], Rie Hasebe[1, 3, #], Shintaro Hojyo[1, 4, #], Yukatsu Shichibu[5, 6, #], Asuka Ishii[1, 7], Yuki Tanaka[1, 4], Kazuki Tainaka[4, 8], Shimpei I. Kubota[1, 4], Katsuaki Konishi[5, 6], and Masaaki Murakami[1, 3, 4, 9, *]

[1]Division of Molecular Psychoneuroimmunology, Institute for Genetic Medicine, Graduate School of Medicine, Hokkaido University, Sapporo, Hokkaido, Japan
[2]Microbiology Department, Faculty of Veterinary Medicine, Alexandria University, Alexandria, Alexandria, Egypt
[3]Division of Molecular Neuroimmunology, Department of Homeostatic Regulation, National Institute for Physiological Sciences, National Institutes of Natural Sciences, Okazaki, Aichi, Japan
[4]Group of Quantum Immunology, Institute for Quantum Life Science, National Institute for Quantum and Radiological Science and Technology, Chiba, Chiba, Japan
[5]Graduate School of Environmental Science, Hokkaido University, Sapporo, Hokkaido, Japan
[6]Faculty of Environmental Earth Science, Hokkaido University, Sapporo, Hokkaido, Japan
[7]Graduate School of Medicine, Medical Sciences, Hokkaido University, Sapporo, Hokkaido, Japan
[8]Department of System Pathology for Neurological Disorders, Brain Research Institute, Niigata University, Niigata, Niigata, Japan
[9]Institute for Vaccine Research and Development (HU-IVReD), Hokkaido University, Sapporo 001-0020, Hokkaido, Japan
*For correspondence: murakami@igm.hokudai.ac.jp
#Contributed equally to this work

Abstract

Microinflammation enhances the permeability of specific blood vessel sites through an elevation of local inflammatory mediators, such as interleukin (IL)-6 and tumor necrosis factor (TNF)-α. By a two-dimensional immunohistochemistry analysis of tissue sections from mice with experimental autoimmune encephalomyelitis (EAE), an animal model for multiple sclerosis (MS), we previously showed that pathogenic immune cells, including $CD4^+$ T cells, specifically accumulate and cause microinflammation at the dorsal vessels of the fifth lumbar cord (L5), resulting in the onset of disease. However, usual pathological analyses by using immunohistochemistry on sections are not effective at identifying the microinflammation sites in organs. Here, we developed a new three-dimensional visualization method of microinflammation using luminescent gold nanoclusters (AuNCs) and the clear, unobstructed brain/body imaging cocktails and computational analysis (CUBIC) tissue-clearing method. Our protocol is based on the detection of leaked AuNCs from the blood vessels due to an enhanced vascular permeability caused by the microinflammation. When we injected ultrasmall coordinated Au_{13} nanoclusters intravenously (i.v.) to EAE mice, and then subjected the spinal cords to tissue clearing, we detected Au signals leaked from the blood vessels at L5 by light sheet microscopy, which enabled the visualization of complex tissue structures at the whole organ level, consistent with our previous report that microinflammation occurs specifically at this site. Our method will be useful to specify and track the stepwise development of microinflammation in whole organs that is triggered by the recruitment of pathogenic immune cells at specific blood vessels in various inflammatory diseases.

Keywords: Experimental autoimmune encephalomyelitis (EAE), $CD4^+$ T cells, Myelin oligodendrocyte glycoprotein (MOG), Gateway reflex, Microinflammation, CUBIC, Au_{13} nanoclusters

This protocol was validated in: Cell (2012), DOI: 10.1016/j.cell.2012.01.022

Background

Multiple sclerosis (MS) is a chronic inflammatory disease of the central nervous system (CNS), mediated by myelin-specific autoreactive $CD4^+$ T cells (International Multiple Sclerosis Genetics et al., 2011). Active experimental autoimmune encephalomyelitis (aEAE) is a well-established animal model of MS that is induced by immunizing mice with myelin oligodendrocyte protein–derived peptide (MOG) and complete Freund's adjuvant (CFA) together with pertussis toxin (PTx). However, where and how pathogenic $CD4^+$ T cells enter the CNS from peripheral blood and cause the disease had been unclear, since it was believed that the CNS is protected from immune cells by the blood–brain barrier (Liu et al., 2012). Using a passive transfer model of EAE, in which pathogenic $CD4^+$ T cells including autoreactive $CD4^+$ T cells from the secondary lymphoid tissues of aEAE mice are transferred to naïve mice, we demonstrated that sensory-sympathetic crosstalk, triggered by gravity stimulation via the soleus muscle, leads to the accumulation of pathogenic immune cells at the dorsal vessels of the fifth lumbar cord (L5) locally, which in turn causes microinflammation, a chronic inflammation that enhances the permeability of specific blood vessel sites by elevated local inflammatory mediators, such as IL-6 and TNF-α (Arima et al., 2012). Importantly, this permeability enables autoreactive $CD4^+$ T cells to enter the CNS. We named this specific neuro-immune interaction the *gateway reflex* and have since demonstrated it can be activated by six types of environmental stimuli: gravity, electricity, pain, stress, light, and inflammation (Arima et al., 2012, 2015 and 2017; Hasebe et al., 2022; Murakami et al., 2019; Stofkova et al., 2019).

Coordinated gold nanoclusters (AuNCs) have an atomically precise molecular structure, ultrasmall size, facile surface modification, and characteristic optical properties (Jin et al., 2016). Some AuNCs have been reported to exhibit unique photoluminescence emission with long lifetimes and large Stokes shift from the visible to near-infrared wavelengths (Chen et al., 2015; Yu et al., 2019), as well as high compatibility and photostability. Thus, they are good candidates as luminophores for long-term imaging, high-sensitivity detection, and target-specific treatment (Luo and Liu, 2022; Palmal and Jana, 2014; Zhang et al., 2022). The usefulness of AuNCs as fluorescent probes has already been shown in imaging, detection, and therapy. Phosphine-coordinated AuNCs represent a luminescent gold cluster family (Konishi et al., 2018; Sugiuchi et al., 2017). Among them, diphosphine-coordinated Au_{13} nanoclusters with an icosahedral gold core motif are interesting, because of their easy accessibility, robustness, and moderately intense photoluminescence in the near-infrared region (Shichibu and Konishi, 2010; Sugiuchi et al., 2015).

The development of tissue-clearing reagents and protocols, efficient fluorescent labeling, and rapid volumetric imaging by light sheet microscopy has enabled new tissue-clearing methods for the 3D imaging of intact tissues and even entire organisms (Hama et al., 2015; Ueda et al., 2020). Despite tissue-clearing approaches enabling high tissue transparency within a few days using organic chemicals (e.g., benzyl alcohol and benzyl benzoate), concerns about the quenching of fluorescent proteins and safety have remained. In response, Tainaka et al. (2014) developed the hydrophilic unobstructed brain/body imaging cocktails and computational analysis (CUBIC) tissue-clearing method, which efficiently removes lipids, pigments, and calcium phosphate to retain the fluorescent signals and enable whole-body imaging with single-cell resolution in mice. Combining light sheet microscopy and CUBIC can visualize rare cells and complex structures in various tissues at the whole organ level.

Chronic microinflammation is a hallmark of many inflammatory diseases, including autoimmune, neurodegenerative, and metabolic syndrome–driven diseases. In such inflammatory diseases with stochastic and proliferative processes, single-cell events ultimately affect the health status of the entire organism. Therefore, a detection system that enables quick identification of the development and progression of microinflammation is desired. However, conventional protocols for identifying inflammation sites are mainly based on 2D histology using inflammatory mediator-specific reporter mice or antibodies, which makes it difficult to accurately identify the sites depending on the tissue sections.

In this protocol, we show a rapid 3D-imaging method to detect microinflammation in aEAE mice using Au_{13} nanoclusters and CUBIC. Au_{13} signals leaked out from the blood vessels around the L5, indicating enhanced vascular permeability caused by microinflammation, supporting our previous findings of a vascular gate formed for pathogenic immune cells to enter the CNS in this region (Arima et al., 2012). Thus, our method is useful for studying the stepwise development of microinflammation at the whole organ level in various inflammatory diseases and will also provide future perspectives of Au_{13} nanocluster-based imaging techniques to study biological events, which are

induced by the enhancement of vascular permeability at specific vessel sites.

Materials and Reagents

1. C57BL/6NCrSlc mice (6–8-week-old male; Japan SLC)
2. 50 mL polypropylene conical tube (Corning, Falcon®, catalog number: 352070)
3. 15 mL polypropylene conical tube (Corning, Falcon®, catalog number: 352096)
4. 1 mL syringe for tuberculin slip tip (TERUMO, catalog number: SS-01T)
5. Injection needle 25G × 1 (TERUMO, catalog number: NN-2525R)
6. Insulin syringe (with 27G × 1/2 needle) (TERUMO, catalog number: SS-10M2713)
7. Normal winged needle for vein D type (25G × 5/8 needle) (TERUMO, catalog number: SV-25DLK)
8. Three-way stopcock (TERUMO, catalog number: TS-TL1K)
9. 30 mL syringe lock type 30 (TERUMO, catalog number: SS-30LZ)
10. 5 mL Costar Stripette (Corning, catalog number: 4487)
11. 10 mL Costar Stripette (Corning, catalog number: 4488)
12. 25 mL Costar Stripette (Corning, catalog number: 4489)
13. MOG_{35-55} (MEVGWYRSPFSRVVHLYRNGK, Sigma-Aldrich)
14. Incomplete Freunds' adjuvant (IFA) (Sigma-Aldrich, catalog number: F5506)
15. *Mycobacterium tuberculosis* H37RA (DIFCO, catalog number: 231141)
16. PTx from *Bordetella pertussis* (Sigma-Aldrich, catalog number: P7208-50UG)
17. Saline (Otsuka Pharmaceutical, catalog number: K6E85)
18. Isoflurane (Pfizer)
19. Sodium chloride (NaCl) (Sigma-Aldrich, catalog number: S9625)
20. Potassium chloride (KCl) (Kanto Chemical, catalog number: 32326-00)
21. Disodium hydrogen phosphate (Na_2HPO_4) (Nacalai Tesque, catalog number: 31801-05)
22. Potassium dihydrogen phosphate (KH_2PO_4) (Kishida Chemical, catalog number: 000-63955)
23. 2-[4-(2-Hydroxyethyl)-1-piperazinyl]ethanesulfonic acid (HEPES) (Sigma-Aldrich, catalog number: H4034)
24. Sodium hydroxide (NaOH) (FUJIFILM Wako Chemicals, catalog number: 198-13765)
25. 4% paraformaldehyde phosphate buffer solution (PFA) (Nacalai Tesque, catalog number: 09154-85)
26. Triton X-100 (Sigma-Aldrich, catalog number: T8787)
27. Sodium azide (FUJIFILM Wako Chemicals, catalog number: 197-11091)
28. Casein from bovine milk (Sigma-Aldrich, catalog number: C3400)
29. 1,2-Hexanediol (Tokyo Chemical Industry, catalog number: H0688)
30. 1-Methylimidazole (Tokyo Chemical Industry, catalog number: M0508)
31. 2,3-Dimethyl-1-phenyl-5-pyrazolone (Tokyo Chemical Industry, catalog number: D1876)
32. Nicotinamide (Tokyo Chemical Industry, catalog number: N0078)
33. Silicone oil (Shin-Etsu Silicone, catalog number: HIVAC-F4)
34. Mineral oil (Sigma-Aldrich, catalog number: M8410-1L)
35. Anti-actin, α-smooth muscle (α-SMA)–FITC antibody, mouse monoclonal (clone: 1A4) (Sigma-Aldrich, catalog number: F3777)
36. Purified rat anti-mouse CD31 (clone: MEC 13.3) (BD Biosciences, catalog number: 550274)
37. Goat anti-rat IgG (H+L) cross-absorbed secondary antibody, Alexa Fluor™ 555 (Thermo Fisher Scientific, catalog number: A-21434)
38. Dimethyl sulfoxide (DMSO) for spectrochemical analysis (FUJIFILM Wako Chemicals, catalog number: 045-28335)
39. Sodium borohydride ($NaBH_4$) (Tokyo Chemical Industry, catalog number: S0480)
40. Ethanol (Kanto Chemical, catalog number: 14033-00)
41. [1,2-Bis(diphenylphosphino)ethane]dichlorodigold(I) ($Au_2(dppe)Cl_2$) (Sigma-Aldrich, catalog number: 717363)
42. Dichloromethane (Kanto Chemical, catalog number: 10158-81)

43. Hydrochloric acid (FUJIFILM Wako Chemicals, catalog number: 080-01061)
44. Acetone (Kanto Chemical, catalog number: 01026-81)
45. Methanol (Kanto Chemical, catalog number: 25183-81)
46. $[Au_{13}(dppe)_5Cl_2]Cl_3$ (Au_{13}) [synthesized according to the literature (Shichibu and Konishi, 2010), see Recipes]
47. 1 M HEPES buffer, pH 7.2 (see Recipes)
48. Phosphate buffered saline (PBS) (see Recipes)
49. Delipidation/decoloration buffer (see Recipes)
50. Staining buffer (see Recipes)
51. CUBIC-R (see Recipes)
52. Observation oil (see Recipes)

Equipment

1. Micro-dissecting scissors (Hammacher, catalog number: HSB014-11)
2. Micro scissors 105 mm straight sword (AS ONE, catalog number: YS-7105)
3. Angled serrated tip forceps (Hammacher, catalog number: HSC187-11)
4. KFI tweezers GG (Kowa Forceps Industry, catalog number: K-3 GG)
5. PIPETMAN P (Gilson, model: P20, catalog number: F123600)
6. PIPETMAN P (Gilson, model: P200, catalog number: F123601)
7. PIPETMAN P (Gilson, model: P1000, catalog number: F123602)
8. Pipet-aid (FALCON/catalog number: 357590)
9. Light sheet microscopy (LaVision BioTec/UltraMicroscope II)
10. Shake-LR (TAITEC, catalog number: 0054809-000)
11. Wave-SI (TAITEC, catalog number: 0054334-000)
12. Double shaker NR-30 (TAITEC, catalog number: 0000205-000)
13. Neo shaker NS-LR (AS ONE, catalog number: 2-7827-01)
14. Stereomicroscope (OLYMPUS, model: SZ61)
15. LED illuminator stand (OLYMPUS, model: SZ2-ILST)
16. Refractive index measurement equipment (ATAGO, catalog number: PAL-RI)

Software

1. Imaris version 9.0.0 (Bitplane, https://imaris.oxinst.com)

Procedure

Figure 1 shows an overview of the protocol.

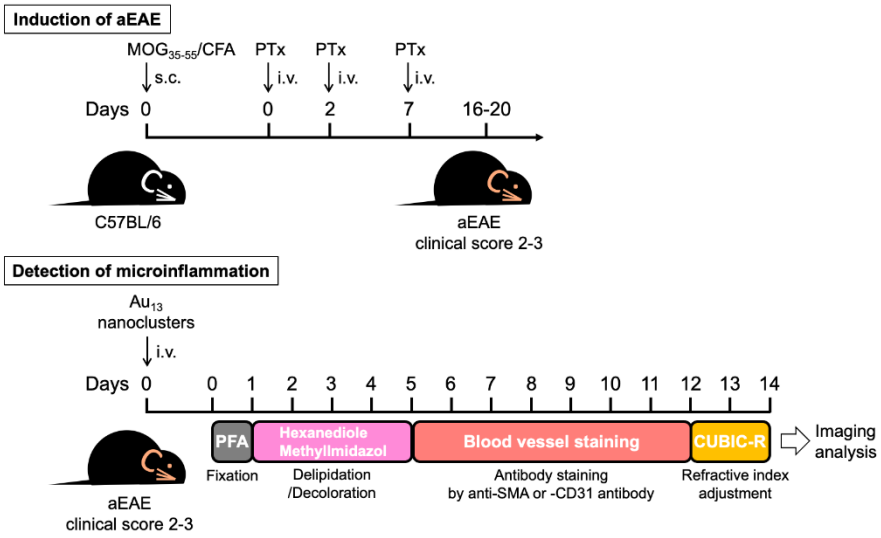

Figure 1. Overview of procedures for microinflammation detection using Au_{13} nanoclusters and the CUBIC tissue-clearing method. Mice were immunized with MOG_{35-55}/CFA (IFA containing *M. tuberculosis* H37RA) and underwent PTx injection. On days 16–20, when experimental autoimmune encephalomyelitis (EAE) develops with clinical scores of 2–3, the EAE mice were injected with Au_{13} nanoclusters, anesthetized after 2 h, and transcardially perfused with PBS and then PFA. The spine with the ribs was taken out and further subjected to PFA fixation for one day. Then, L1–L6 were excised carefully and immersed in delipidation/decoloration reagent (hexanediol/methylimidazole) for four days (days 1–5). After delipidation and decoloration, L1–L6 were stained with anti-SMA or anti-CD31 for seven days (days 5–12) and subjected to refractive index adjustment in CUBIC-R (days 12–14). The Au signal was visualized by light sheet microscopy and analyzed by Imaris software.

A. Induction of EAE

1. Mix 100 µL (400 µg) of 4 mg/mL of MOG_{35-55} in PBS and 100 µL of CFA [10 mL of IFA plus two vials (20 mg) of *M. tuberculosis* H37RA] in two syringes using a three-way stopcock. Emulsify by pressing the syringe back and forth, transferring the contents from one syringe to the other for 5–10 min until a stable white emulsion is produced (for details, see Tanaka et al., 2017).
2. Immunize C57BL/6 mice with 200 µL of MOG_{35-55}/CFA subcutaneously (s.c.) at the tail base using a 1 mL syringe with a 25G needle on day 0.
3. Inject i.v. 400 ng of PTx in 200 µL of saline into the tail vein of mice using an insulin syringe on days 0, 2, and 7.
4. Assess clinical scores of EAE daily with a 0–5 scoring system (0, no signs; 1, flaccid tail; 2, impaired righting reflex and/or gait; 2.5, paralysis of one hind limb; 3, paralysis of both hind limbs; 4, hind limb paralysis with partial fore limb paralysis; 5, moribund or dead).

B. Preparation of Au_{13} nanoclusters

1. Synthesize Au_{13} nanoclusters ($[Au_{13}(dppe)_5Cl_2]Cl_3$; see Recipe 1) and isolate as crystalline solids according to the procedures described in Shichibu and Konishi (2010).
2. Store 160 µM Au_{13} nanoclusters in DMSO.

C. Fixation of spines from Au_{13} nanoclusters–treated EAE mice

1. Prior to injecting into mice, Au_{13} nanoclusters are diluted 5-fold with 10 mM HEPES (pH 7.2, see Recipe 2) or saline to 32 μM.
2. Inject i.v. 200 μL of 32 μM Au_{13} nanoclusters into the tail vein of aEAE mice with clinical score 2–3 using the insulin syringe.
3. After 2 h, anesthetize the mice with 4% isoflurane.
4. Perfuse the mice with PBS (see Recipe 3) and PFA using the winged needle and three-way stopcock locked by syringes.
   a. Make an incision in the right atrial appendage of the heart.
   b. Perfuse with 25 mL of cold PBS via the left ventricle of the heart using the syringe with the 25G winged needle.
   c. After the PBS perfusion, change the solution to 4% PFA using the three-way stopcock.
5. Perfuse with 20 mL of cold 4% PFA.
6. Take out the spine with the ribs (Video 1) and immerse in 40 mL of 4% PFA in a 50 mL tube at 4 ℃ for 24 h with shaking at 60 rpm in an orbital motion on a TAITEC Shake-LR.

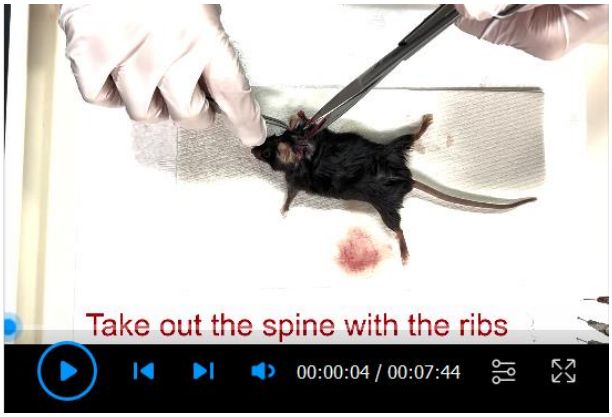

Video 1. Procedures for the L1-L6 preparation. After transcardial perfusion with PBS followed by PFA, the spine with the ribs was immediately taken out and further fixed with PFA. Then, L1–L6 were excised by carefully cutting the intervertebral discs between T13-L1 and L6-S1 with a razor, with the T13 rib as a position marker under stereomicroscopy installed with an LED illuminator.

D. Delipidation/decoloration

1. Wash the spine with the ribs with 40 mL of PBS at room temperature for 30 min three times while shaking at 30 rpm in a seesaw motion on a TAITEC Wave-SI.
2. Excise L1–L6 carefully under stereomicroscopy installed with the LED illuminator (Video 1).
3. Immerse L1–L6 in 40 mL of delipidation/decoloration buffer (see Recipe 4) in a 50 mL tube at 37 ℃ for 4 days with shaking at 80 rpm in a reciprocating motion on an AS ONE Neo shaker NS-LR.

E. Antibody staining

1. Wash L1–L6 with 40 mL of PBS at room temperature for 1 h three times with shaking at 30 rpm in a seesaw motion on the TAITEC Wave-SI.
2. Dilute FITC-conjugated α-SMA antibody and purified rat anti-mouse CD31, which recognize smooth muscle actin on the artery to platelet endothelial cell adhesion molecule-1 on whole blood vessels, respectively, to 1:50 in staining buffer (see Recipe 5).

3. Immerse L1–L6 in 1.5 mL of the diluted antibody solution in a 5 mL polypropylene tube at room temperature for seven days with light shielding and shaking at 100 rpm in an orbital motion on the TAITEC double shaker NR-30.
4. Wash L1–L6 with 40 mL of PBS in a 50 mL tube at room temperature for 30 min three times with light shielding and shaking at 30 rpm in a seesaw motion on the TAITEC Wave-SI.
5. For anti-CD31 staining:
   a. Further immerse L1–L6 in 1.5 mL of Alexa Fluor 555-conjugated goat anti-rat IgG diluted to 1:200 in staining buffer at room temperature for two days with light shielding and shaking at 100 rpm in an orbital motion on the TAITEC double shaker NR-30.
   b. Wash L1–L6 with 40 mL of PBS in a 50 mL tube at room temperature for 30 min three times with light shielding and shaking at 30 rpm in a seesaw motion on the TAITEC Wave-SI.
6. Postfix L1–L6 with 10 mL of 1% PFA in PBS at room temperature for 5 h with light shielding and shaking at 30 rpm in a seesaw motion on the TAITEC Wave-SI.
7. Wash L1–L6 with 40 mL of PBS at room temperature for 30 min three times with light shielding and shaking at 30 rpm in a seesaw motion on the TAITEC Wave-SI.

F. Refractive index adjustment

Living organisms are composed of molecules with different refractive indices, such as water, proteins, and lipids. In order to observe mammalian tissues in 3D by light sheet microscopy, it is important to suppress light scattering by making the refractive index uniform.

1. Immerse L1–L6 in 10 mL of 1/2 CUBIC-R [diluted CUBIC-R (see Recipe 6) to 1:1 in dH_2O] at room temperature for 5 h with light shielding and shaking at 100 rpm in an orbital motion on the TAITEC double shaker NR-30.
2. Discard 1/2 CUBIC-R and immerse L1–L6 in 10 mL of CUBIC-R at room temperature overnight with light shielding and shaking at 100 rpm in an orbital motion on the TAITEC double shaker NR-30.
3. Replace with fresh CUBIC-R and further immerse L1–L6 at room temperature for 4 h with light shielding and shaking at 100 rpm in an orbital motion on the TAITEC double shaker NR-30 (Figure 2).

Figure 2. Cleared lumbar cords. Brightfield image of the lumbar cords before and after tissue clearing.

G. Microscopy and image analysis

1. Wash L1–L6 with 10 mL of observation oil (see Recipe 7).
2. Place L1–L6 into a glass container filled with observation oil.
3. Acquire 3D images using a light sheet microscope (UltraMicroscope II) as reported previously (Dodt et al., 2007; Susaki et al., 2014).

4. Collect all raw image data in lossless 16-bit TIFF format.
5. Visualize, capture, and analyze 3D-rendered images using Imaris software, version 9.0.0 (Figures 3 and 4, Videos 2 and 3).

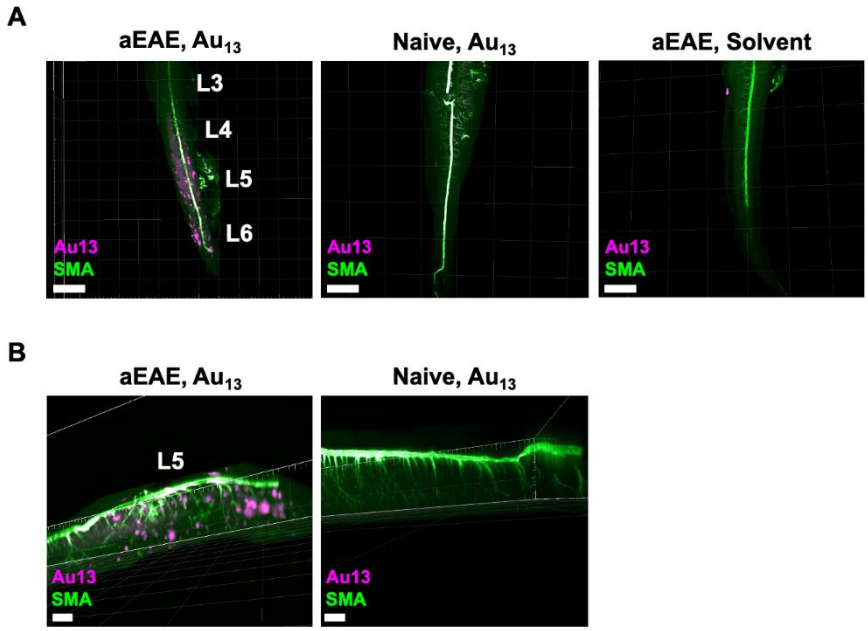

Figure 3. Detection of microinflammation at L5 by Au_{13} nanoclusters and staining of the artery with anti-SMA antibody. (A) aEAE mice with clinical score 2.5 and naïve mice were injected i.v. with Au_{13} nanoclusters or solvent. Figures show cleared L3–L6 from each mouse stained with anti-SMA antibody, which recognizes smooth muscle actin on the artery. The signal of Au_{13} nanoclusters was visualized as a punctate signal with a diameter of 50–200 nm in the dorsal blood vessels centered on L5 and in the parenchyma of the spinal cords in aEAE mice. Intravascular Au signals were also observed in aEAE and naïve mice injected with Au_{13} nanoclusters. Scale bars, 1,500 μm. Magenta: Au_{13} nanocluster; green: SMA (artery). (B) Magnified images of L5 from the aEAE and naïve mice in (A). Scale bars, 1,000 μm. Magenta: Au_{13} nanocluster; green: SMA (artery).

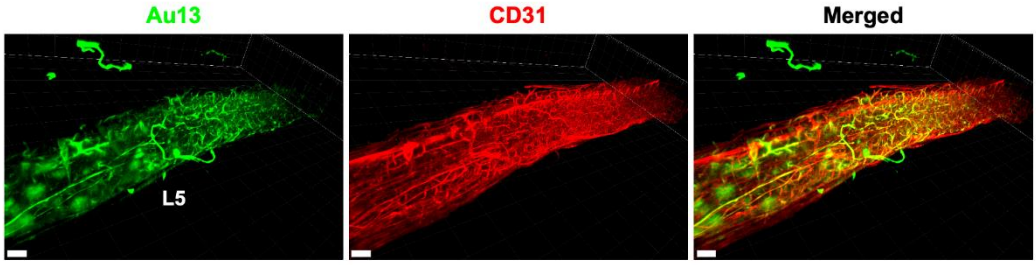

Figure 4. Detection of microinflammation at L5 by Au_{13} nanoclusters and staining of whole blood vessels with anti-CD31 antibody. aEAE mice with clinical score 3 were injected i.v. with Au_{13} nanoclusters. Cleared L5 stained with anti-CD31 antibody, which recognizes platelet endothelial cell adhesion molecule-1 on whole blood vessels, is shown. Scale bars, 400 μm. Green: Au_{13} nanocluster; red: CD31 (blood vessel).

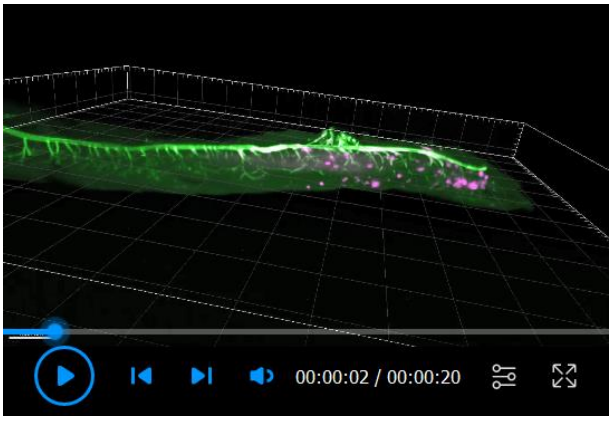

Video 2. The detection of microinflammation at L5 by Au_{13} nanoclusters and staining of the artery with anti-SMA antibody. A 3D movie of the lumbar spinal cords of an aEAE mouse with clinical score 2.5 after injecting i.v. with Au_{13} nanoclusters. The cleared lumbar spinal cords were stained with anti-SMA antibody, which recognizes smooth muscle actin on the artery. Magenta: Au_{13} nanocluster; green: SMA (artery).

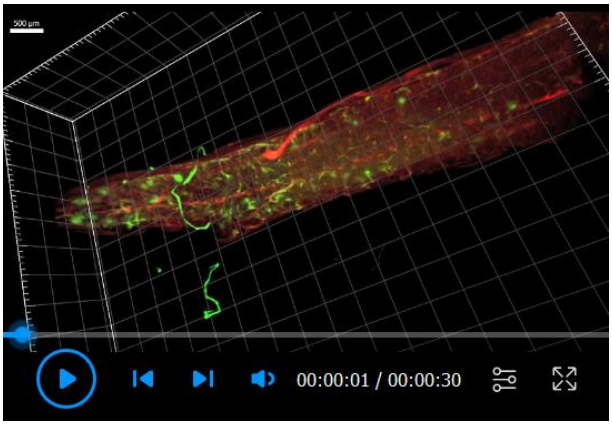

Video 3. The detection of microinflammation at L5 by Au_{13} nanoclusters and staining of whole blood vessels with anti-CD31 antibody. A 3D movie of the lumbar spinal cords of an aEAE mouse with clinical score 3 after injecting i.v. with Au_{13} nanoclusters. The cleared lumbar spinal cords were stained with anti-CD31 antibody, which recognizes platelet endothelial cell adhesion molecule-1 on whole blood vessels. Green: Au_{13} nanocluster; red: CD31 (blood vessel).

Notes

1. Sodium azide–containing staining buffer is classified as a particularly hazardous substance due to high acute toxicity, especially to dermis.
2. CUBIC-R and other reagents are safe reagents, so there is no need to prepare them under a chemical fume hood. Further, they are highly stable and not difficult to prepare.
3. The injection of 200 µL of PTx or Au_{13} nanoclusters i.v. should be performed by slowly pressing the insulin syringe and injecting the full volume of solution for approximately five seconds.
4. In our aEAE induction protocol, the disease usually develops with clinical scores of 2–3 on days 16–20 after the immunization. However, the timing of the disease onset and when the clinical score reaches 2–3 may depend on the manufacturing lot of the MOG peptides, CFA, and PTx as well as the mouse age and sex.

5. Mice with clinical score 3–4 were humanely euthanized according to ethical regulations.
6. When Au_{13} nanoclusters were injected for 4 h, the Au signal was not detected. Therefore, we set the time to 2 h.
7. Mice were anesthetized with 4% isoflurane and PBS was then perfused while the mice were alive. Since the end of the transcardial perfusion uses 25 mL of PBS (more than 10 times the total blood volume), the mice were dead before the PFA perfusion.
8. In the fixation, washing, and refractive index adjustment steps, the entire tissue sample may be transferred from a decanter to a clean container and then transferred again into a tube filled with fresh buffer or solution using tweezers without a hook or spoon to minimize damage.
9. In step D2, L1–L6 should be excised from the spine carefully to minimize damage using micro-scissors and angled serrated tip forceps under the stereomicroscope with illuminator (Video 1).
10. The compounds used for delipidation/decolorization are surfactants and may affect antigenicity.
11. The lumbar spinal cords are regularly immersed in delipidation/decoloration buffer only once.
12. From step E3 onward, the samples should be protected from light.
13. For step E3, a 1.5 mL Eppendorf tube may be a bit small. For the spinal cord, a 2 mL tube is fine for antibody staining.
14. For light sheet microscopy, pictures are taken so that all tissues are included. It is recommended to acquire data in Z-stacks every 5 µm.
15. In our protocol, the spots were not counted. However, it would be possible to count visually or calculate the volume of each spot with a software such as Imaris.

Recipes

1. $[Au_{13}(dppe)_5Cl_2]Cl_3$ (Au_{13})

Synthesize and isolate as crystalline solids according to the method of Shichibu and Konishi (2010).

a. Add 10 mL of ethanol containing $NaBH_4$ (66.2 mg, 1.75 mmol) to 240 mL of dichloromethane containing $Au_2(dppe)Cl_2$ (302 mg, 0.35 mmol).
b. Stir the mixture at room temperature for 3 h.
c. Remove the solvent, suspend the residue in dichloromethane, and filter.
d. Evaporate the filtrate to dryness until forming a dark-brown powder (283.6 mg).
e. Dissolve the powder in ethanol (49 mL) and then treat with 1 mL aqueous hydrochloric acid (12 mmol).
f. Stir the mixture at room temperature for 24 h.
g. Evaporate the volatiles.
h. Wash the resulting residue with acetone.
i. Suspend the resulting residue in methanol and filter.
j. Evaporate the filtrate to dryness until forming $[Au_{13}(dppe)_5CI_2]CI_3$ (Au_{13}) as crystalline red solids (75.9 mg).
k. Weigh the crystalline solids of the Au_{13} cluster (~3 mg).
l. Dissolve the crystalline solids in dimethyl sulfoxide (final concentration: 160 µM).
m. Store the nanoclusters at room temperature for up to one month with light shielding.

2. 1 M HEPES buffer, pH 7.2 (1,000 mL)

a. Add 238.3 g of HEPES to 800 mL of dH_2O.
b. Adjust the buffer to pH 7.2 with 10 N NaOH.
c. Add dH_2O up to 1,000 mL (final concentration: 1 M).
d. To prepare 10 mM HEPES buffer, 1 M HEPES buffer is diluted 100-fold with dH_2O.
e. Store the buffer at room temperature for up to one month.

3. PBS (1,000 mL)

a. Add the following substances to 800 mL of dH_2O:
   8 g of NaCl (final concentration: 137 mM)
   0.2 g of KCl (final concentration: 2.68 mM)
   1.15 g of Na_2HPO_4 (final concentration: 8.1 mM)
   0.2 g of KH_2PO_4 (final concentration: 1.47 mM)
b. Add dH_2O up to 1,000 mL.
c. Store PBS at room temperature for up to one month.

4. Delipidation/decoloration buffer (500 g)

a. Add the following substances to 440 g of PBS:
   50 g of 1,2-Hexanediol [final concentration: 10% (w/w)]
   10 g of 1-Methylimidazole [final concentration: 2% (w/w)]
b. Store the buffer at room temperature for up to one month.

5. Staining buffer (100 mL)

a. Mix the following substances and add dH_2O up to 100 mL:
   5 mL of 10% Triton X-100 in dH_2O (final concentration: 0.5%)
   0.1 mL of 10% sodium azide in dH_2O (final concentration: 0.01%)
   5 mL of 20× PBS (final concentration: 1×)
   50 mL of 1% casein in PBS (final concentration: 0.5%; should be resolved to make 1% solution in PBS by warming at 60 ℃)
b. Store the buffer at 4 ℃ for up to one month.

6. CUBIC-R (500 g)

a. Add the following substances to 125 mL dH_2O:
   225 g of 2,3-Dimethyl-1-phenyl-5-pyrazolone [final concentration: 45% (w/w)]
   150 g Nicotinamide [final concentration: 30% (w/w)]
b. Store CUBIC-R at room temperature for up to one month with light shielding.

7. Observation oil (100 g; refractive index = 1.52, 25 ℃)

a. Add the following substances to a 100 mL tube and shake gently:
   60.2 g of silicone oil (HIVAC-F4) (Refractive index = 1.555, 25 ℃)
   39.8 g of mineral oil (Refractive index = 1.467, 25 ℃)
b. Measure the refractive index using a refractometer and adjust by adding either oil to 1.52.
c. Store the oil at room temperature for up to one month.

Acknowledgments

We appreciate the excellent technical assistance and secretarial assistance provided by Ms. C. Nakayama, Ms. S. Takano, Ms. S. Fukumoto, Ms. N. Yamamoto, Ms. S. Morita, and Ms. M. Ohsawa. We also thank Dr. Peter Karagiannis for proofreading the text. This work was supported by KAKENHI (MM, HR, SH, SIK), Japan Science and Technology Agency (JPMXS0120330644 (Q-Leap)), Japan Agency for Medical Research and Development (AMED) (MM; JP21zf0127004 and JP223fa627005), and the Takeda Science Foundation (MM, SH). This study was also supported partly by the Grant for Joint Research Program of the Institute for Genetic Medicine, Hokkaido University, by the Photo-Excitonix Project, Hokkaido University, and by the Promotion Project for Young Investigators at Hokkaido University (MM). This protocol is based on our previous experimental procedures for EAE induction (Arima et al., 2012; Ogura et al., 2008; Tanaka et al., 2017), Au_{13} nanocluster preparation (Shichibu and Konishi, 2010), and CUBIC tissue-clearing protocol (Tainaka et al., 2014).

Competing interests

The authors declare no competing interests.

Ethics

All animal experiments described herein were approved by the Institutional Animal Care and Use Committees of the Institute for Genetic Medicine, Hokkaido University, and were performed according to institutional guidelines and regulations.

References

Arima, Y., Harada, M., Kamimura, D., Park, J. H., Kawano, F., Yull, F. E., Kawamoto, T., Iwakura, Y., Betz, U. A., Marquez, G., et al. (2012). Regional neural activation defines a gateway for autoreactive T cells to cross the blood-brain barrier. *Cell* 148(3): 447-457.

Arima, Y., Kamimura, D., Atsumi, T., Harada, M., Kawamoto, T., Nishikawa, N., Stofkova, A., Ohki, T., Higuchi, K., Morimoto, Y., et al. (2015). A pain-mediated neural signal induces relapse in murine autoimmune encephalomyelitis, a multiple sclerosis model. *Elife* 4: e08733.

Arima, Y., Ohki, T., Nishikawa, N., Higuchi, K., Ota, M., Tanaka, Y., Nio-Kobayashi, J., Elfeky, M., Sakai, R., Mori, Y., et al. (2017). Brain micro-inflammation at specific vessels dysregulates organ-homeostasis via the activation of a new neural circuit. *Elife* 6: e25517.

Chen, L. Y., Wang, C. W., Yuan, Z. and Chang, H. T. (2015). Fluorescent gold nanoclusters: recent advances in sensing and imaging. *Anal Chem* 87(1): 216-229.

Dodt, H. U., Leischner, U., Schierloh, A., Jahrling, N., Mauch, C. P., Deininger, K., Deussing, J. M., Eder, M., Zieglgansberger, W. and Becker, K. (2007). Ultramicroscopy: three-dimensional visualization of neuronal networks in the whole mouse brain. *Nat Methods* 4(4): 331-336.

Hama, H., Hioki, H., Namiki, K., Hoshida, T., Kurokawa, H., Ishidate, F., Kaneko, T., Akagi, T., Saito, T., Saido, T., et al. (2015). ScaleS: an optical clearing palette for biological imaging. *Nat Neurosci* 18(10): 1518-1529.

Hasebe, R., Murakami, K., Harada, M., Halaka, N., Nakagawa, H., Kawano, F., Ohira, Y., Kawamoto, T., Yull, F. E., Blackwell, T. S., Nio-Kobayashi, J., et al. (2022). ATP spreads inflammation to other limbs through crosstalk between sensory neurons and interneurons. *J Exp Med* 219(6): e20212019.

International Multiple Sclerosis Genetics, C., Wellcome Trust Case Control, C., Sawcer, S., Hellenthal, G., Pirinen, M., Spencer, C. C., Patsopoulos, N. A., Moutsianas, L., Dilthey, A., Su, Z., Freeman, et al. (2011). Genetic risk and a primary role for cell-mediated immune mechanisms in multiple sclerosis. *Nature* 476(7359): 214-219.

Jin, R., Zeng, C., Zhou, M. and Chen, Y. (2016). Atomically Precise Colloidal Metal Nanoclusters and Nanoparticles: Fundamentals and Opportunities. *Chem Rev* 116(18): 10346-10413.

Konishi, K., Iwasaki, M. and Shichibu, Y. (2018). Phosphine-Ligated Gold Clusters with Core+ exo Geometries: Unique Properties and Interactions at the Ligand-Cluster Interface. *Acc Chem Res* 51(12): 3125-3133.

Liu, W. Y., Wang, Z. B., Zhang, L. C., Wei, X. and Li, L. (2012). Tight junction in blood-brain barrier: an overview of structure, regulation, and regulator substances. *CNS Neurosci Ther* 18(8): 609-615.

Luo, X. and Liu, J. (2022). Ultrasmall Luminescent Metal Nanoparticles: Surface Engineering Strategies for Biological Targeting and Imaging. *Adv Sci (Weinh)* 9(3): e2103971.

Murakami, M., Kamimura, D. and Hirano, T. (2019). Pleiotropy and Specificity: Insights from the Interleukin 6 Family of Cytokines. *Immunity* 50(4): 812-831.

Ogura, H., Murakami, M., Okuyama, Y., Tsuruoka, M., Kitabayashi, C., Kanamoto, M., Nishihara, M., Iwakura, Y. and Hirano, T. (2008). Interleukin-17 promotes autoimmunity by triggering a positive-feedback loop via interleukin-6 induction. *Immunity* 29(4): 628-636.

Palmal, S. and Jana, N. R. (2014). Gold nanoclusters with enhanced tunable fluorescence as bioimaging probes. *Wiley Interdiscip Rev Nanomed Nanobiotechnol* 6(1): 102-110.

Shichibu, Y. and Konishi, K. (2010). HCl-induced nuclearity convergence in diphosphine-protected ultrasmall gold clusters: a novel synthetic route to "magic-number" Au13 clusters. *Small* 6(11): 1216-1220.

Stofkova, A., Kamimura, D., Ohki, T., Ota, M., Arima, Y. and Murakami, M. (2019). Photopic light-mediated down-regulation of local α_{1A}-adrenergic signaling protects blood-retina barrier in experimental autoimmune uveoretinitis. *Sci Rep* 9(1): 2353.

Sugiuchi, M., Maeba, J., Okubo, N., Iwamura, M., Nozaki, K. and Konishi, K. (2017). Aggregation-Induced Fluorescence-to-Phosphorescence Switching of Molecular Gold Clusters. *J Am Chem Soc* 139(49): 17731-17734.

Sugiuchi, M., Shichibu, Y., Nakanishi, T., Hasegawa, Y. and Konishi, K. (2015). Cluster-pi electronic interaction in a superatomic Au13 cluster bearing sigma-bonded acetylide ligands. *Chem Commun (Camb)* 51(70): 13519-13522.

Susaki, E. A., Tainaka, K., Perrin, D., Kishino, F., Tawara, T., Watanabe, T. M., Yokoyama, C., Onoe, H., Eguchi, M., Yamaguchi, S., et al. (2014). Whole-brain imaging with single-cell resolution using chemical cocktails and computational analysis. *Cell* 157(3): 726-739.

Tainaka, K., Kubota, S. I., Suyama, T. Q., Susaki, E. A., Perrin, D., Ukai-Tadenuma, M., Ukai, H. and Ueda, H. R. (2014). Whole-body imaging with single-cell resolution by tissue decolorization. *Cell* 159(4): 911-924.

Tanaka, Y., Arima, Y., Higuchi, K., Ohki, T., Elfeky, M., Ota, M., Kamimura, D. and Murakami, M. (2017). EAE Induction by Passive Transfer of MOG-specific $CD4^+$ T Cells. *Bio Protoc* 7(13): e2370.

Ueda, H. R., Erturk, A., Chung, K., Gradinaru, V., Chedotal, A., Tomancak, P. and Keller, P. J. (2020). Tissue clearing and its applications in neuroscience. *Nat Rev Neurosci* 21(2): 61-79.

Yu, H. Z., Rao, B., Jiang, W., Yang, S. and Zhu, M. Z. (2019). The photoluminescent metal nanoclusters with atomic precision. *Coordin Chem Rev* 378: 595-617.

Zhang, C., Gao, X., Chen, W., He, M., Yu, Y., Gao, G. and Sun, T. (2022). Advances of gold nanoclusters for bioimaging. *iScience* 25(10): 105022.